CHAPTER – 5

Phase Evolution, Thermal Stability and Indentation Behavior of MgAlSiCrFeCuZn LDHEA Processed through Mechanical Alloying and Spark Plasma Sintering

CHAPTER 5

PHASE EVOLUTION, THERMAL STABILITY AND INDENTATION BEHAVIOR OF MgAlSiCrFeCuZn LOW-DENSITY HIGH ENTROPY ALLOY PROCESSED THROUGH MECHANICAL ALLOYING AND SPARK PLASMA SINTERING

This chapter consists of a detailed study on the synthesis and characterization of an equiatomic MgAlSiCrFeCuZn high entropy alloy by mechanical alloying (MA) route. X-ray diffraction, transmission electron microscopy (TEM), scanning electron microscopy (SEM) were employed to study the phase evolution in milled alloy powder and spark plasma sintered (SPSed) LDHEA. The STEM–EDS mapping has been carried out to confirm the homogenous elemental distribution in milled powders after mechanical alloying. The thermal stability of these LDHEA powders were ascertained through DSC technique. The phases evolved were co-related through the ex-situ XRD of LDHEA powders annealed at various temperatures. Attempts were made to explore the mechanical properties of the LDHEA through instrumented microindentation techniques. The hardness and estimated yield strength value were evaluated and co-related with the phases evolved. The phase evolution and their stability were discussed and attributed to the various thermodynamical parameters as well as other parameters as proposed in the literature.

5.1 Phase evolution during mechanical alloying of MgAlSiCrFeCuZn powder

X-Ray diffraction analysis of mechanically milled sample was carried out at different durations of 1h, 10 h, 30 h, 40 h, and 50 h (Figure 5.1) with a ball to powder ratio of 10:1. The milling sequence is shown from bottom to top. Initially at 1h of milling, all the elements were present and there was no evidence of significant alloying. After 10 h of milling, elemental peaks started disappearing indicating initiation of alloying. It is also observed that low melting point elements like Zn, Al, and Mg were disappearing at faster rate suggesting that these elements are going into lattice of high melting point phase forming elements like Fe and Cr. After 30h of milling, there was a formation of single BCC

phase along with the minor fraction of γ-brass type phase and some undissolved Si. Even after 50h of milling, XRD is showing single silicon peak at lower angle indicating that more milling might be required to completely dissolve Si. This may due to relatively high melting point and completely different crystal structure of Si compared to other constituent element.

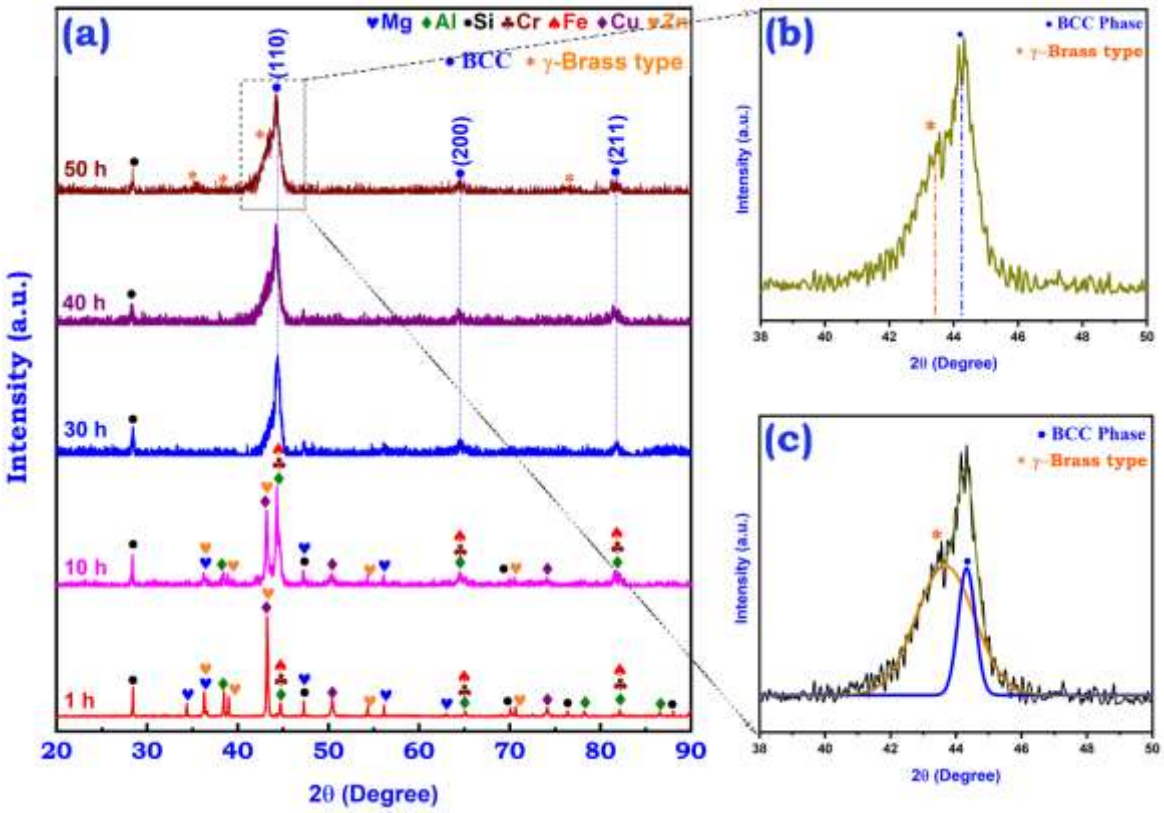

Figure 5.1: Phase evolution after mechanical alloying of MgAlSiCrFeCuZn HEA up to 50 h with BPR of 10:1 (a); Enlarged image showing peak position of (110) peak of BCC and minor phase in 50 h milled powder (b); Deconvoluted peak showing the presence of BCC and γ-brass type phase in 50 h milled powder (c).

Further to understand the dissolution of Si into the solid solution, the ball to powder ratio (BPR) of 20:1 was used for mechanical milling as shown in the Figure 5.2. It was observed that with a BPR of 20:1, the phase fraction of γ-brass type increases in comparison

with the mechanically alloyed powder of BPR of 10:1. In similar line the phase fraction of the Si decreases on increasing the BPR.

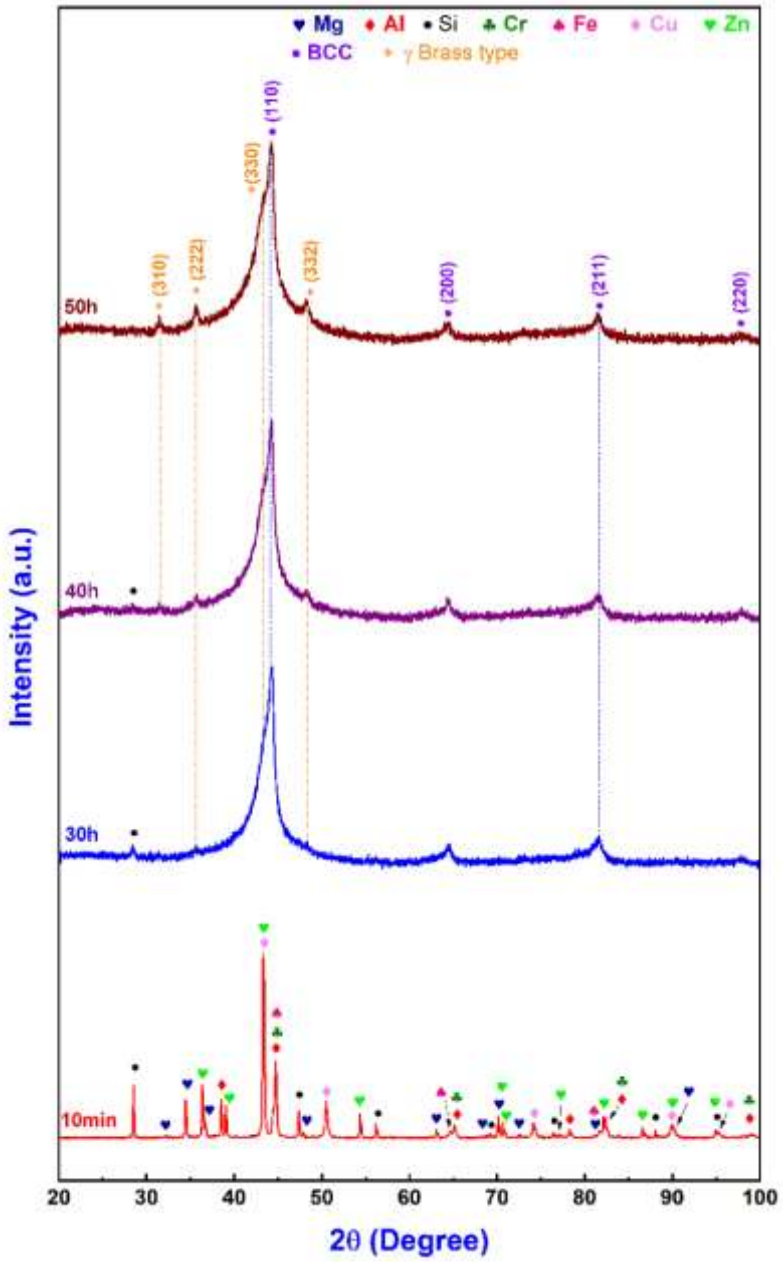

Figure 5.2: Phase evolution during mechanical alloying of MgAlSiCrFeCuZn HEA up to 50 h with BPR of 20:1.

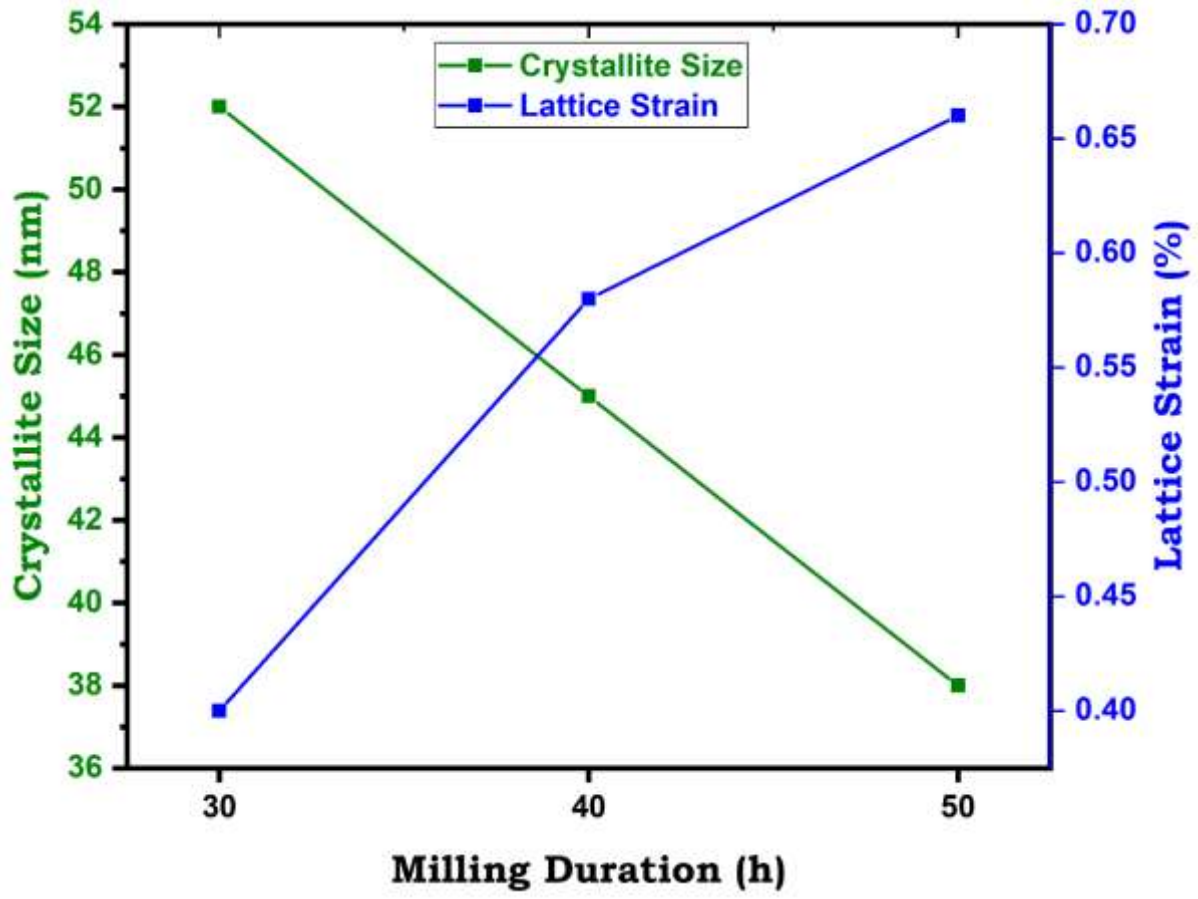

Figure 5.3: Variation of crystallite size and lattice strain as function of milling duration.

Table 5.1: Variation of crystallite size and lattice strain of MgAlSiCrFeCuZn MA high entropy alloy

Sl.No	MILLING TIME (h)	CRYSTALLITE SIZE (nm)	LATTICE STRAIN (%)
1	30	52	0.40
2	40	45	0.58
3	50	38	0.66

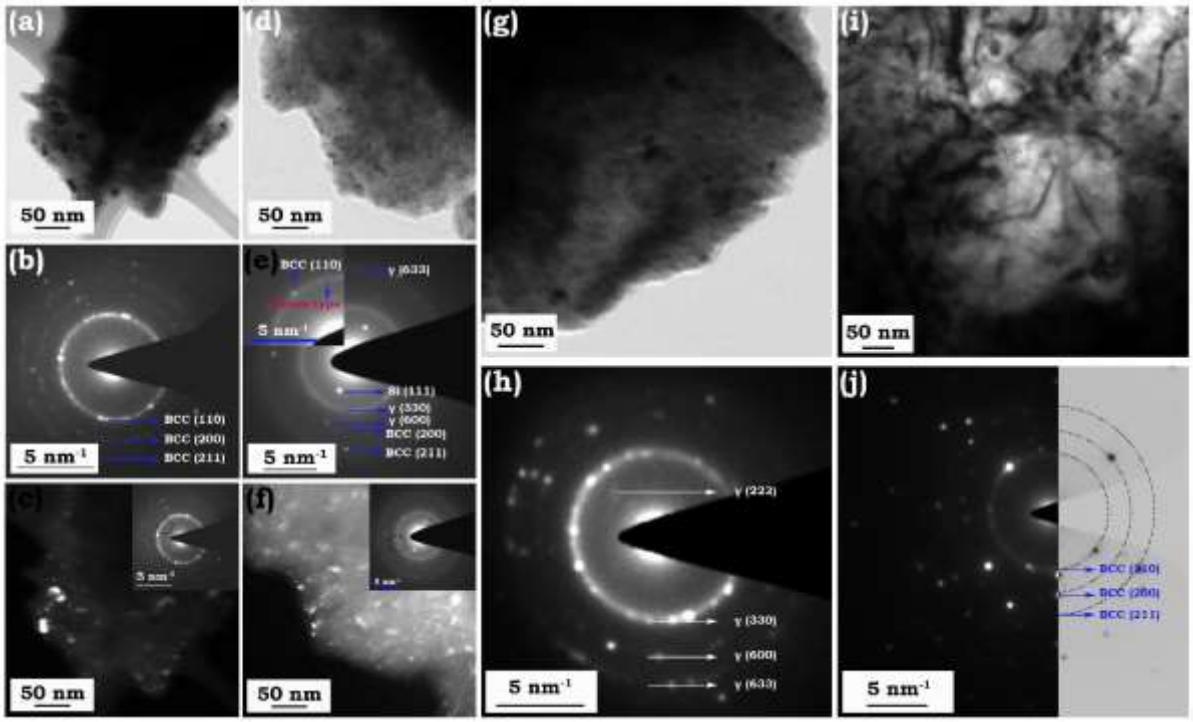

Figure 5.4: TEM micrograph showing fine microstructural details of 50 h milled powder. (a), (b), (c) representing BF, SAD pattern and DF images showing presence of BCC phase; (d), (e) and (f) representing BF, composite SAD pattern and DF images showing co-existence of BCC and γ-brass type phase; (g) and (h) representing BF and SAD pattern of powder particle having only γ-brass type phase; (i) and (j) representing BF and SAD pattern of severely deformed powder particles having BCC phase.

The metallic elements like Mg, Al, Cu, Zn, Cr, and Fe were deformed, cold-welded and fractured during milling. However, Si has a diamond cubic structure with strong covalent bondings, not amenable to easy plastic deformation. Accordingly, the alloying of Si is comparatively less compared to other elements. It is also observed from the XRD pattern that with increase in milling duration, there is broadening of peaks indicating decrease in crystallite size and increase in lattice strain. Precision lattice parameter of the BCC phase was determined to be a=0.2895 ± 0.003 nm.

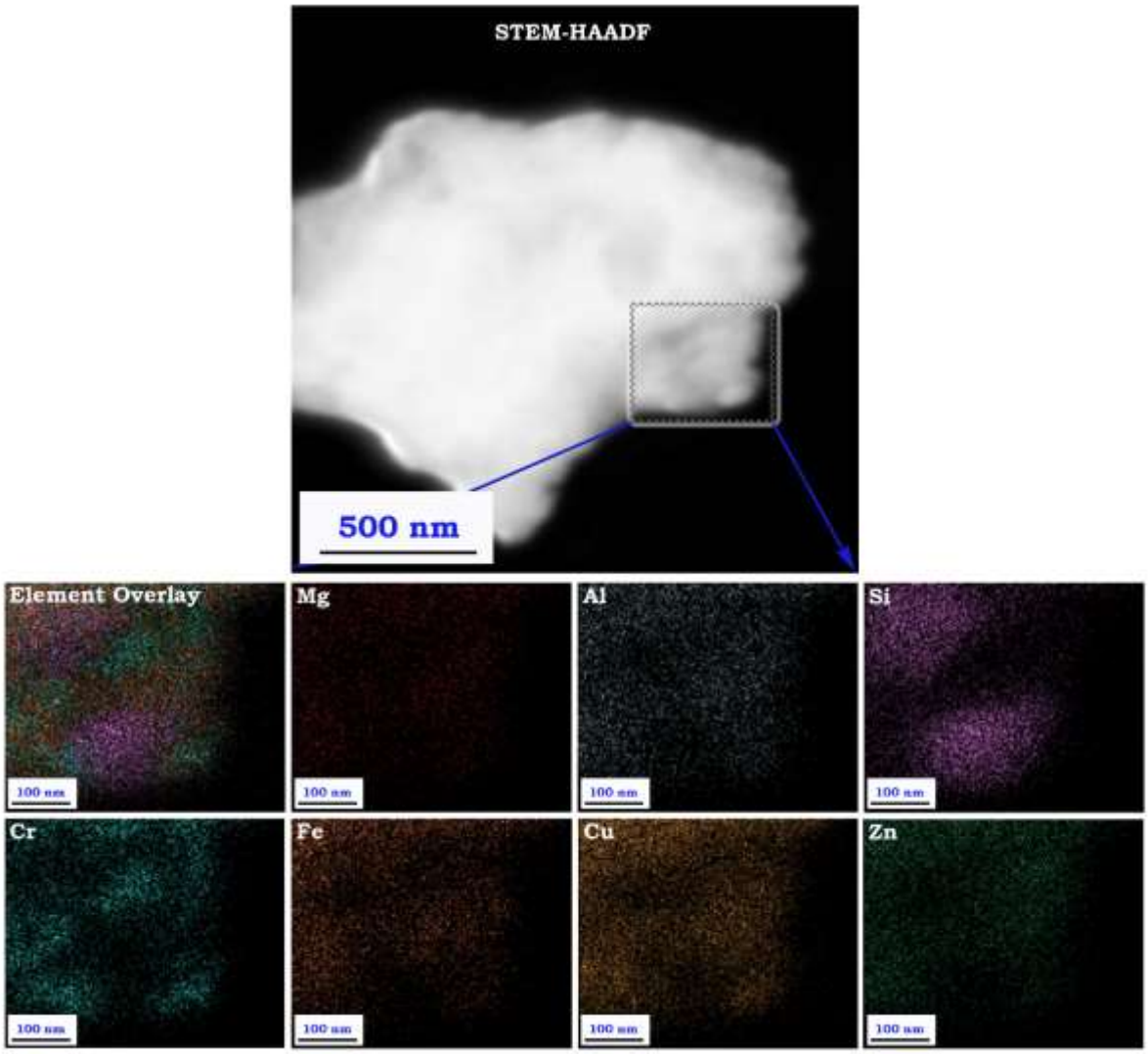

Figure 5.5: STEM-EDS mapping of 50 h milled HEA powder particle.

The lattice strain increase causes a rise in dislocation density. This can be attributed to (i) mismatch in the atomic radius of individual elements (ii) Increase in population density of grain boundaries due to the simultaneous crystal refinement and induced stress by excess free volume of grain boundaries [3, 4], and (iii) mechanical deformation caused by increased dislocation density also enhances the lattice strain and extent of crystallite size refinement as shown in the Figure 5.3.

5.2 Nanostructure nature and elemental mapping of mechanically alloyed powder

The TEM micrograph as shown in the Figure 5.4 represents the formation of nanostructured grains in the MgAlSiCrFeCuZn LDHEA powder milled for 50 h. The bright-field image, selected area diffraction pattern (SADP) and corresponding dark-field image of MgAlSiCrFeCuZn HEA powder are shown in Figure 5.4 (a-c) respectively. The structure and fine microstructural features are identified through TEM micrographs shown in Figure 5.4. The SADP of the 50 h milled powder shows the ring pattern indicating polycrystalline nature of sample corresponding to the (110), (200), (211) diffraction rings of BCC phase. These results are in close agreement with the XRD patterns (Figure 5.1). Bright field and dark field images of MgAlSiCrFeCuZn alloy are shown in Figure 5.4 (a) and (c).

These images are also depicting the formation of nanostructure grains which are in range of 7 nm to 17 nm range. Figure 5.4 (d) to (f) represent BF, composite SAD pattern and DF images respectively showing co-existence of BCC and γ-brass type phase; the presence of γ-brass type phase along with the parent BCC phase may be discerned from the SADP shown in Figure 5.4 (e). This confirms the findings of a minor amount of γ-brass type phase along with a BCC phase in the milled powder. The Figure 5.4 (g) and Figure 5.4 (h) represent BF and SAD pattern of powder particle having only γ-brass type phase; Figure 5(i) and (j) represents BF and SAD pattern of severely deformed powder particle having a BCC type phase.

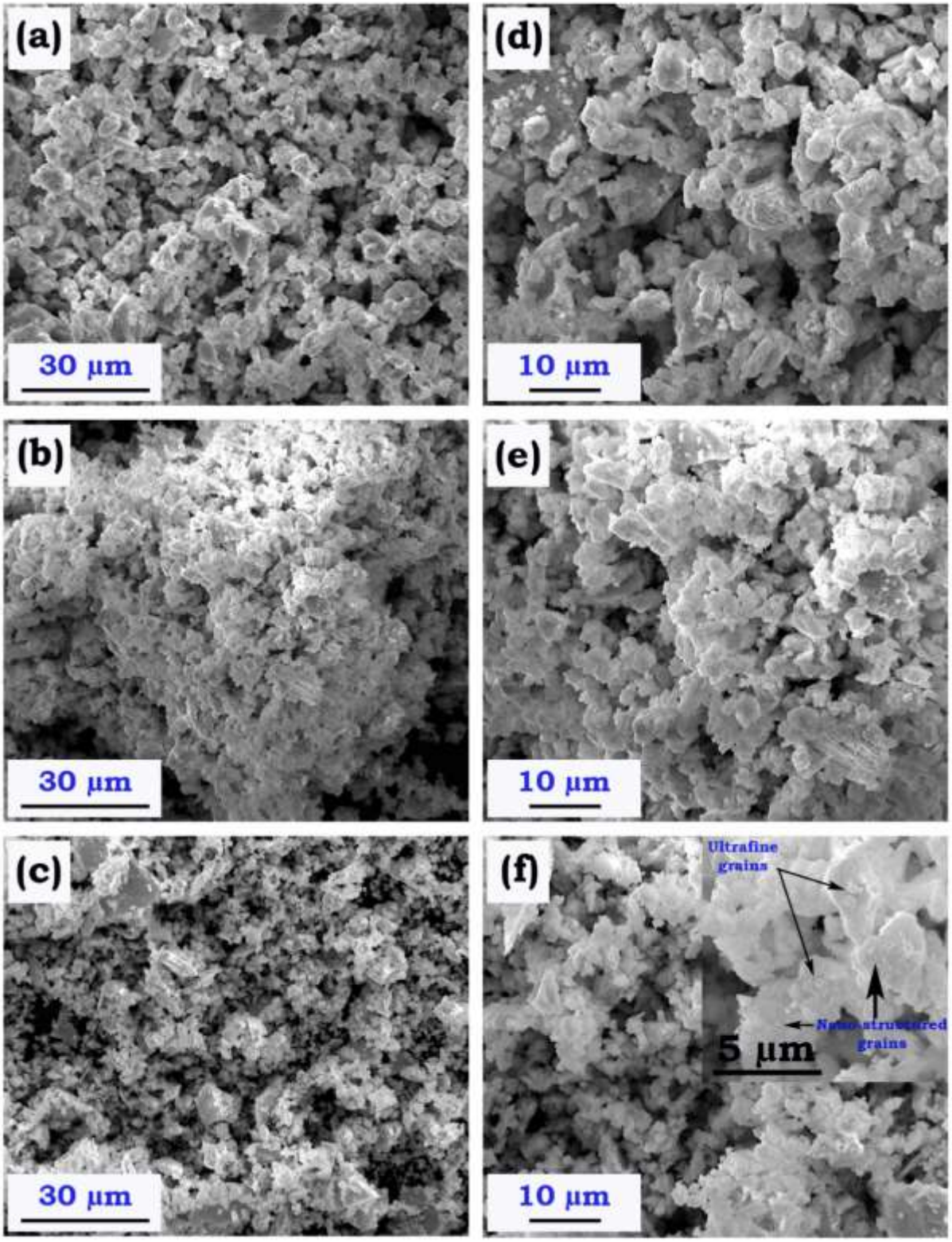

Figure 5. 6: SEM micrograph showing morphology of 30 h (a & d), 40 h (b & e) and 50 h (c & f) milled powder.

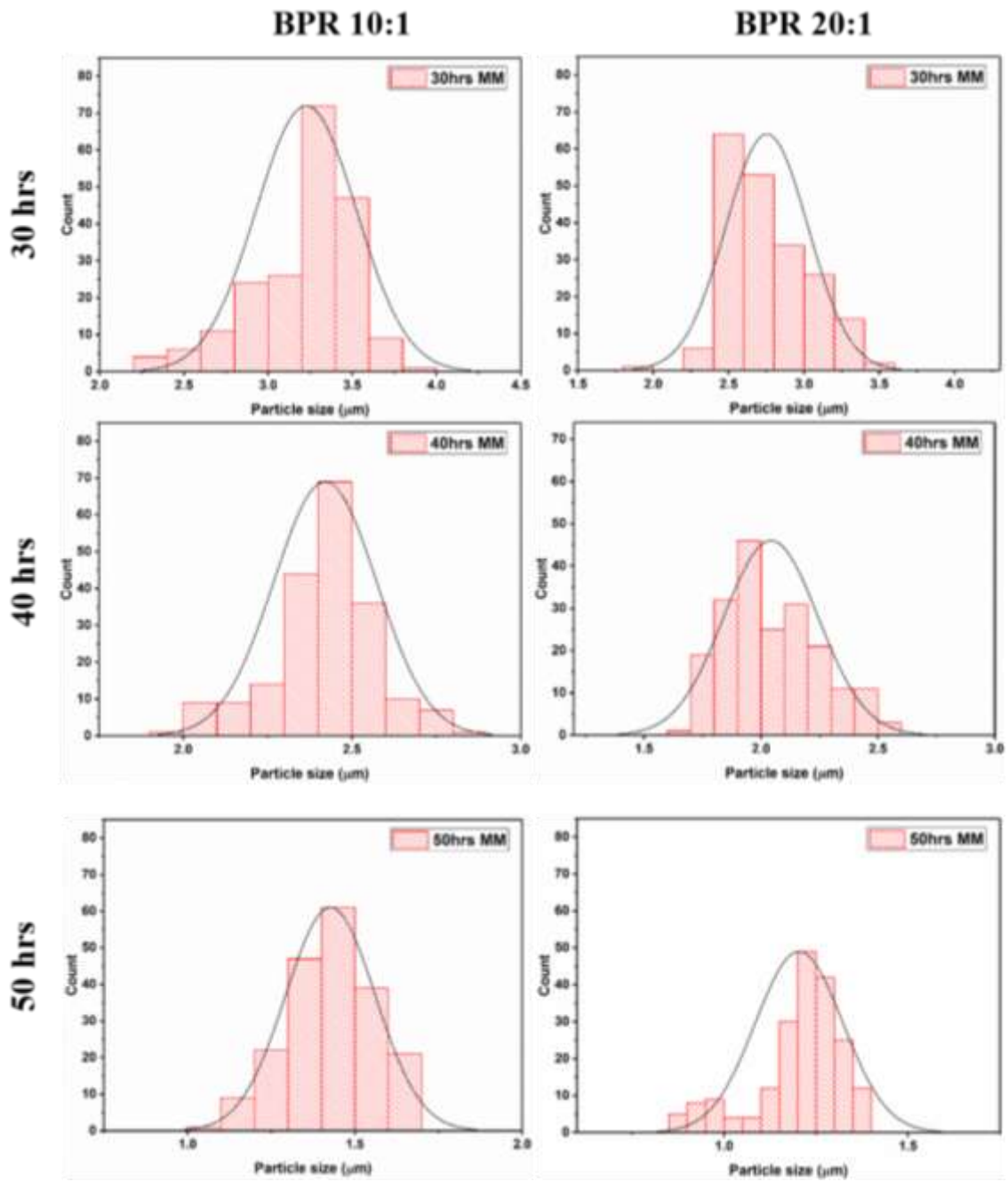

Figure 5.7: Particle size distribution of 50 h mechanically alloyed MgAlSiCrFeCuZn LDHEA with a BPR of 10:1 and 20:1.

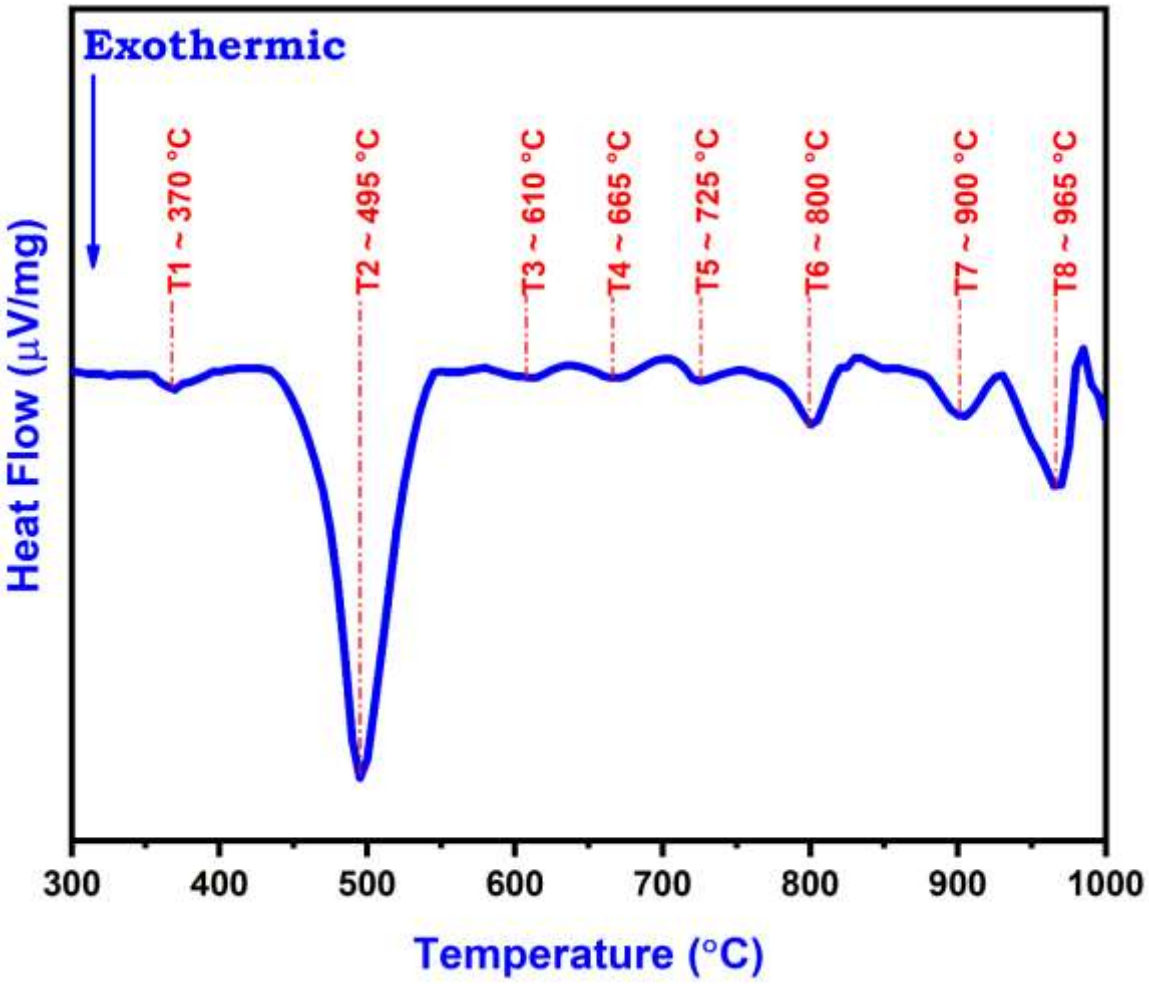

Figure 5.8: DSC thermogram of 50 h milled powder up to 1000 ℃ (1273 K) with scan rate of 20 k.min^{-1}.

The STEM-EDS elemental mapping of 60 h milled powder is displayed in Figure 5.5. The presence of homogeneous distribution of all the elements could be observed with the variation in the intensity of element like Si. The particle having a Si-rich region can be observed as evident from its intensity. The regions rich in Si are found to be lean in Cr, Fe, Cu, Zn, Mg and Al. The STEM–EDS results are in good agreement with the findings of the XRD patterns and TEM results indicating the presence of undissolved Si along with BCC phase.

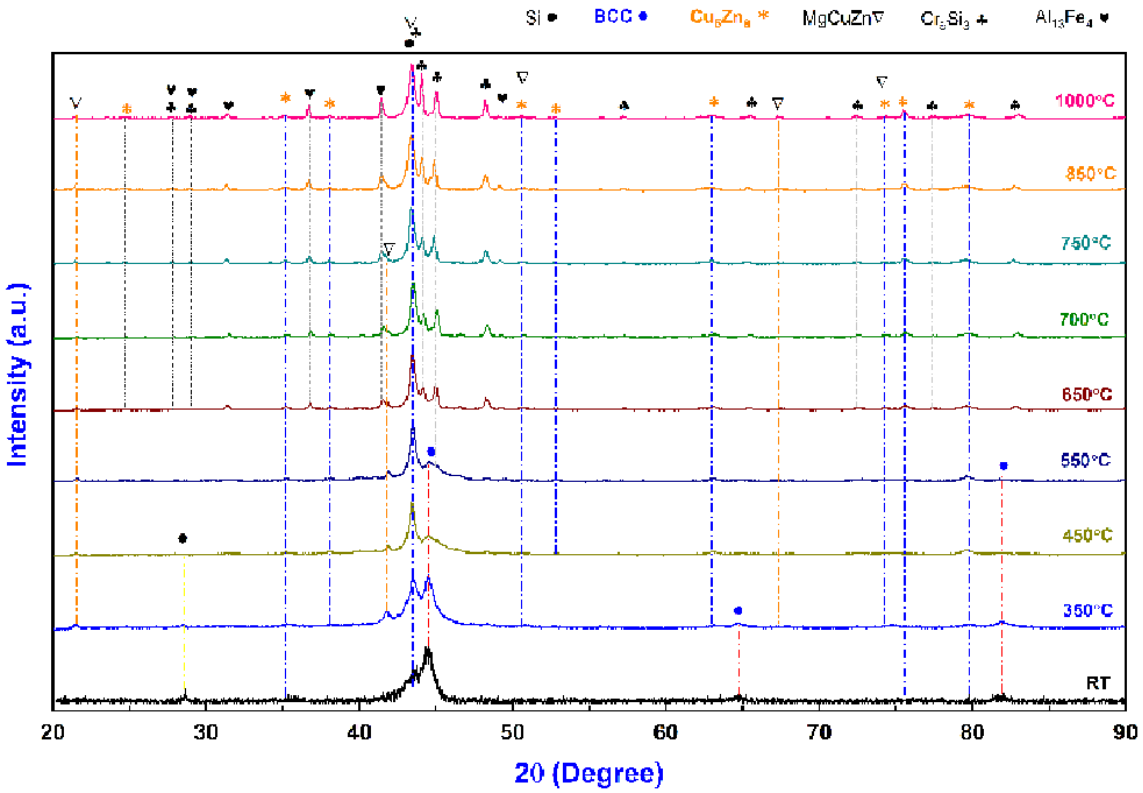

Figure 5.9: Ex-situ XRD of 50 h mechanically alloyed MgAlSiCrFeCuZn LDHEA powder annealed at various temperatures up to 1000 ℃ (1273 K).

5.3 Analysis of powder morphology and thermal stability of the milled powder

The SEM micrographs of Figure 5.6 (a), (b), (c), (d), (e) and (f) show the morphology of the milled powder at various milling time. It may be seen from Figure 5. 6 that the milled particles are irregular in shape as well as non-uniform in size. SEM analysis indicates decrement of powder particle size with time of milled powder for 30 h (a & d), 40 h (b & e) and 50 h (c & f) milled powder respectively. The elemental composition obtained through SEM–EDS analysis is very close to that of the nominal chemical composition. This confirms the homogenous distribution of each element at micrometer length scale. The influence of BPR on the particle size refinement is shown in the Figure 5.7. From the Figure 5.7, it can be discerned that on increasing the duration of milling as well as the ball to powder ratio, the extent of particle size refinement can be achieved to a

greater extent. The particle size of milled powder at 10:1 BPR was found to be ~1.4 µm, while that for 20:1 BPR was ~1.2 µm as evident from Figure 5.7.

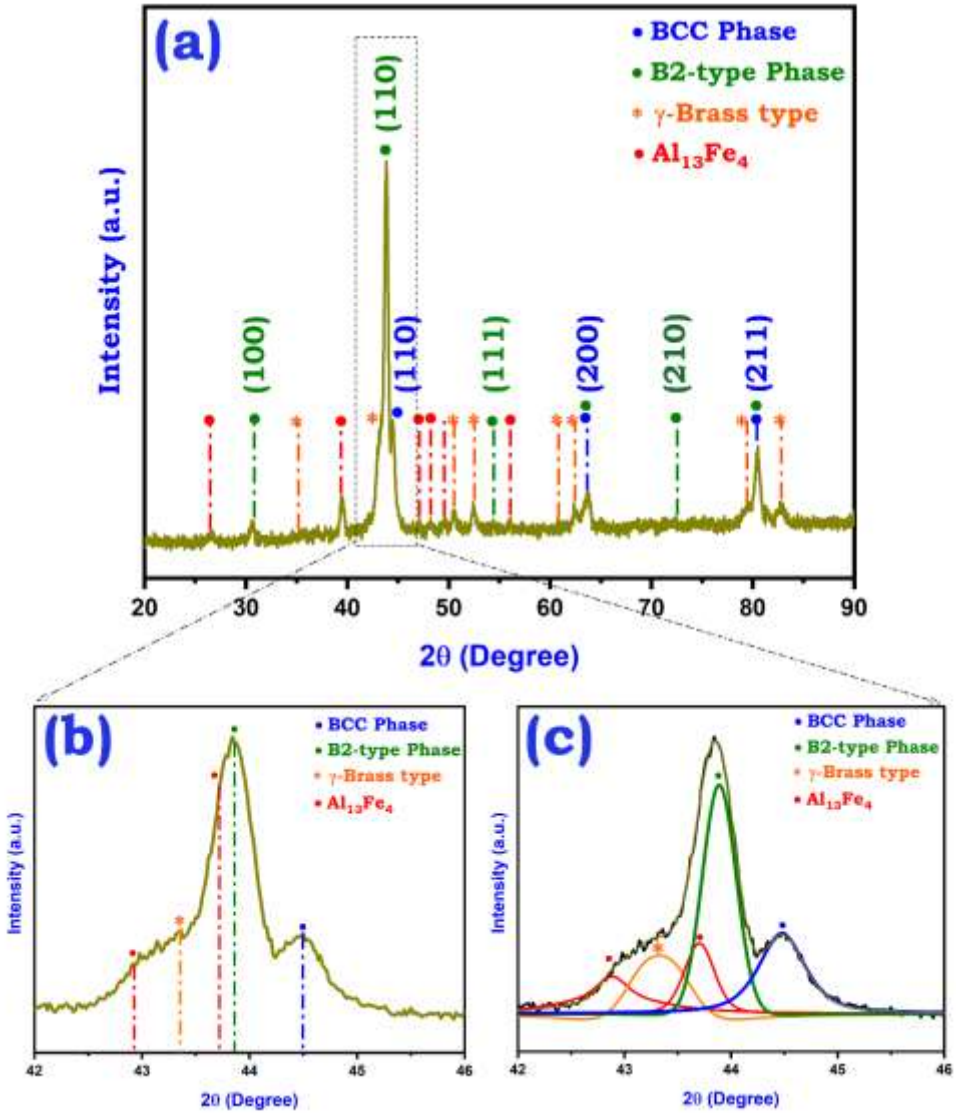

Figure 5.10: Phase formation in MgAlSiCrFeCuZn HEA powder spark plasma sintered at 800 °C (1273 K) for 15 min (a); Enlarged image showing the peak position of BCC/ B2 phase along with other minor phases (b); Expanded image of the deconvoluted peaks for BCC/ B2 phase along with other minor phases (c).

The thermal stability of the milled powder was studied through DSC by heating the powder up to 1200 °C (1473 K) at a scan rate of 20 K.min^{-1} as shown in Figure 5.8. The thermal profile showed exothermic events indicated as T1, T2, T3, T4, T5,T6, T7 and T8

at temperature of 370 ℃ (643 K), 495 ℃ (768 K), 610 ℃ (883 K), 665 ℃ (938 K), 725 ℃ (998 K), 800 ℃ (1073 K), 900 ℃ (1173 K) and 965 ℃ (1230 K) respectively.

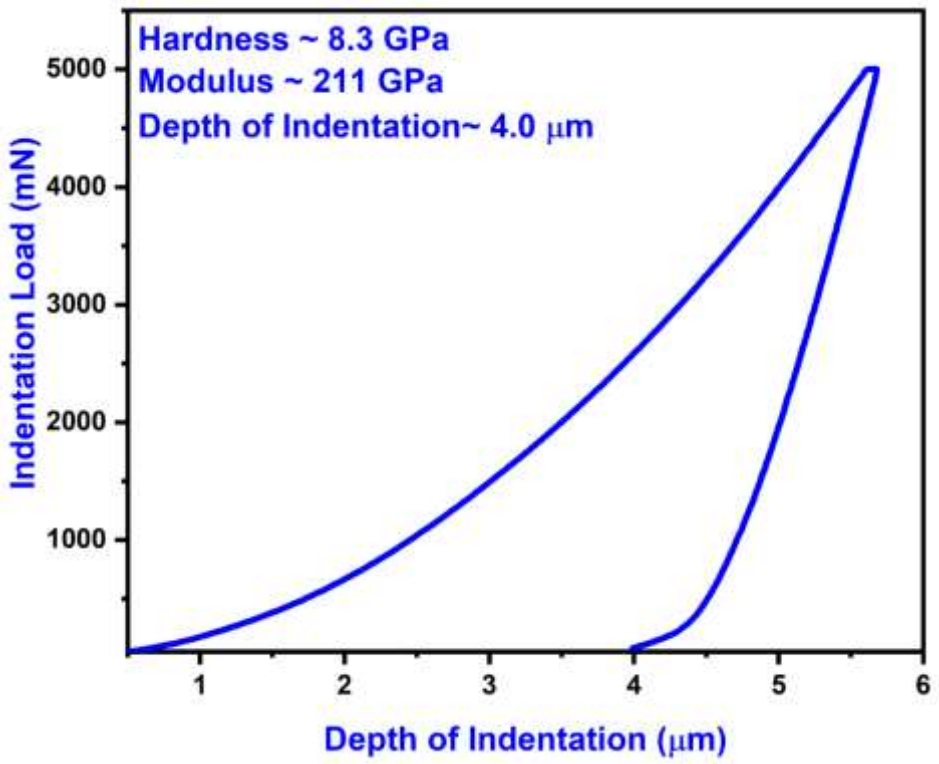

Figure 5.11: Plot showing Indentation load vs depth of indentation for MgAlSiCrFeCuZn LDHEA powder spark plasma sintered at 800 ℃ (1273 K) for 15 min.

The heating events correspond to the phase transformation taking place during heating of HEA powder particles. The phases corresponding to the heating events can be understood with the help of ex-situ XRD of annealed powders at various temperature up to 1000 ℃ as shown in the Figure 5.9. The heating events correspond to the evolution of phases i.e. γ-brass, Cr_5Si_3, MgCuZn (a=b=0.5069 nm, c=0.7169; tP12), and $Al_{13}Fe_4$.

5.4 Phase evolution and mechanical properties of the SPSed LDHEA

The phase evolution after spark plasma sintering of MgAlSiCrFeCuZn HEA powder at 800 ℃ (1073 K) for 15 min has been ascertained through ex-situ XRD

experiments. The parent BCC phase was able to survive along with the B2 type phase. Apart from these two major phases, a minor amount of intermetallics was also observed. The minor phases, such as $Al_{13}Fe_4$, and γ-brass type formed after SPS is marked in Figure 5. 10 (a). The (110) peak of the BCC phase was exploded to show the minor phases illustrated in Figure 5.10 (b). The intense peak of γ-brass and $Al_{13}Fe_4$ [i.e, (620) (d~0.2101 nm), (332) (d~0.2094) and (025) (d~0.2048 nm)] and other minor phases are systematically marked in Figure 5.10 (b). The (110) peak of the BCC phase was deconvoluted, as shown in Figure 5.10 (c). The deconvoluted peaks represent the (110) peak of BCC and B2 phases respectively. The goodness of fit for (110) peak of BCC and B2 phase was ≥95%, while the minor phases are not of as significant as their goodness of fit was not good.

Table 5.2: Mechanical properties of SPSed MgAlSiCrFeCuZn LDHEA.

Sample	SPS Temperature	Mechanical Properties		
		Hardness (GPa)	Modulus (GPa)	Estimated Yield Strength (GPa)
MgAlSiCrFeCuZn	800 ℃	8.38	211	2.8

The LDHEA sample prepared by SPS has appreciable microhardness as mentioned in Table 5.2. The MgAlSiCrFeCuZn SPSed sample's microhardness is 8.3 ± 0.31 GPa, and modulus of elasticity is 211 GPa. Yield strength has been found to be 2.8 GPa (Estimated YS = Hardness/3). These superior mechanical properties of these LDHEAs can make them a candidate material for lightweight structural applications.

Table 5.3: Chemical enthalpy of mixing (ΔH_{ij}^{mix}, kJ/mol) of atomic pairs for MgAlSiCrFeCuZn LDHEA following the Miedema's approach [5].

Elements	**Mg**	**Al**	**Si**	**Cr**	**Fe**	**Cu**	**Zn**
Mg	-	-2	-26	24	18	-3	-4
Al	-2	-	-10	-11	-11	-1	1
Si	-26	-2	-	-37	-35	- 19	-18
Cr	24	-10	-37	-	-1	12	5
Fe	18	-11	-35	-1	-	13	4
Cu	-4	-22	-40	-7	-2	-	1
Zn	- 4	1	-18	5	4	1	-

5.5 Discussion

In contrast to the conventional alloys, solid solution formation can take place in the central region of phase diagram, provided high entropy effect can negate the other unfavorable situation. Phase formation in HEAs can be discussed further on the basis of the parameters such as enthalpy of mixing, the entropy of mixing, the atomic size difference, valence electron concentration etc. The enthalpy of mixing of the septenary MgAlSiCrFeCuZn HEA as calculated by regular solution model [152] has been found to be – 8.98 kJ/mol. Binary values of enthalpy of mixing were calculated by Miedema model, displayed in Table 5.3 [153,154]. The entropy of mixing by Boltzmann hypothesis is evaluated to be 11.50 J/mol/k [36]. Atomic size difference parameter, δ introduced by Zhang et al. [36] was found to be around 8.2%. According to prediction rule for solid-solutions to be formed in multicomponent alloys, the proposed values of the enthalpy of

mixing and the entropy of mixing should lie in the interval -22 to 7 kJ/mol and 11 to19.5 J/mol/k respectively, while the atomic size difference should be less than 8.5% [153,154]. The alloy system selected here satisfies all the three required parameters. Another parameter, Ω is defined [36] to predict the solid solution formation in HEAs and valence electron concentration (VEC) [35,152] to predict structure were calculated and found to be 1.39 and 6.5 respectively. Ω represents the ratio between the entropy and enthalpy of the system. As defined by Zhang et al. [36], $\Omega \geq 1$ supports the solid solution and $\Omega < 1$ supports intermetallic phase formation in multicomponent alloys. Smaller (<6.87) and larger (>8) VEC favors stability of BCC and FCC phases, respectively [36]. In our alloy system, we found $\Omega > 1$ and VEC < 6.87, so they support the formation of BCC solid solution. For HEAs it has been proposed that if $\Omega > 1$, then the contribution of $T\Delta S_{mix}$ will be more than that of ΔH_{mix} and HEAs will be a solid solution and if $\Omega < 1$, then ΔH_{mix} will be a dominant part, thus resulting in formation of intermetallic compounds in HEAs system.

Formation of a single BCC phase with some undissolved Si can be observed at 30 h of milling. Si is having DC structure which is different from other elements. XRD pattern indicated faster disappearance of low melting point elements like Mg, Al, and Zn. This can be suggested due to faster diffusion rates of these elements owing to their low activation energy barrier as compared to that of other high melting point elements like Fe, Cu and Si. Additionally, lattice defects introduced during milling process may also enhance the pace of alloy formation. However, even after 50 h of MA, there is still some undissolved Si present along with BCC phase suggesting the need for further milling. Based on the experimental results, it is concluded that 50 h milling of MgAlSiCrFeCuZn HEA leads to the formation of a major and minor phases associated with BCC (Fe) solid solution and DC (Si), respectively. The order in which the phases evolve are dependent on the physical

parameters of constituent elements of equi-atomic HEA, given in Table 5.3. In principle, melting point, atomic radii and self-diffusion coefficients can in principle decide the order of phase evolution. Higher melting points elements have higher bond strength and stability in comparison with the elements with a low melting point and therefore it can act as a host lattice for HEA. Considerable role is played by self-diffusion coefficient in deciding the phase evolution sequence. All the above factors govern the sequence in which phases evolve during the MA of MgAlSiCrFeCuZn HEA. Cr has highest melting point among all the other elements used. Similarly, Mg possess the highest self-diffusion coefficient and Si, the lowest among all the elements used.

Shivam et al. [150,154–156] have shown the role played by melting point of individual elements for their special affinity to form host lattice, during the systematic investigation of phase evolution in a few equiatomic and non-equatomic HEAs composition. The sequence depends on the bond strength of the elements used in the HEA. They have also found the presence of minor phases of Mn along with the Fe and Cr host lattice after completion of MA. Similar to the present case, Maulik et al. [64,158] have also shown the presence of two BCC phases with increase in mole fraction of Mg (x=1.0, 1.7). Maulik et al. [64,158] have justified the sequence of phase evolution on the basis of bond strength as a function of melting point, atomic radii and self-diffusion coefficient. In spite of having lower melting point than Fe and Cr, Si is able to maintain its identity even after 50 h of MA, which may be due to its lower diffusion coefficient and non-metallic character. The high hardness may be attributed to grain refinement, solid solution strengthening and precipitation hardening.

5.6 Conclusions

The following conclusions can be made from the present chapter:

1. An equiatomic MgAlSiCrFeCuZn HEA was successfully synthesized through mechanical alloying. Mechanically alloyed powder exhibited a major solid solution phase of BCC structure (a= 0.2895 ± 0.003 nm) along with the minor fraction of γ-brass type phase (a=0.878 ± 0.002 nm). A minor amount of Si (~5 %) was found to be undissolved.
2. The increase in the ball to powder ratio from 10:1 to 20:1 decreases the fraction of undissolved Si and enhances the particle size refinement of the LDHEA powders. Nanocrystalline nature (size of ~15 nm) of 60 h milled MgAlSiCrFeCuZn LDHEA powder with a BCC phase and small amount of γ-brass type phase (a=0.878 ± 0.002 nm) was confirmed by TEM. The alloy is observed to be thermally stable up to a temperature of ~400 ℃ (673 K).
3. The positive enthalpy of mixing of binary Mg-Cr, Mg-Fe, and high negative enthalpy of mixing among other elements are unfavorable for the stability of a single- solid solution phase. Hence, it has led to a number of several phases after sintering. Thus, alloy design for HEAs appears to be a challenging task for developing a single-phase solid solution in this hepternary multicomponent alloy system.
4. The SPSed LDHEA exhibited a significant BCC and B2 phases along with a minor amount of other phases i.e., $Al_{13}Fe_4$ and γ-brass phases. The SPSed LDHEA sample showed very high value of hardness and modulus of elasticity of ~8.38 and 211 GPa respectively due to the co-existence of B2-type, $Al_{13}Fe_4$ phase, along with parent BCC phase in the SPSed LDHEA.